Molecular Cell
Article

Quantitative Analysis of Pathways Controlling Extrinsic Apoptosis in Single Cells

John G. Albeck,[1] John M. Burke,[1,2] Bree B. Aldridge,[1,2] Mingsheng Zhang,[1] Douglas A. Lauffenburger,[2] and Peter K. Sorger[1,2,*]
[1]Department of Systems Biology, Harvard Medical School, WAB Room 438, 200 Longwood Avenue, Boston, MA 02115, USA
[2]Center for Cell Decision Processes, Department of Biological Engineering, Massachusetts Institute of Technology, Cambridge, MA 02139, USA
*Correspondence: peter_sorger@hms.harvard.edu
DOI 10.1016/j.molcel.2008.02.012

SUMMARY

Apoptosis in response to TRAIL or TNF requires the activation of initiator caspases, which then activate the effector caspases that dismantle cells and cause death. However, little is known about the dynamics and regulatory logic linking initiators and effectors. Using a combination of live-cell reporters, flow cytometry, and immunoblotting, we find that initiator caspases are active during the long and variable delay that precedes mitochondrial outer membrane permeabilization (MOMP) and effector caspase activation. When combined with a mathematical model of core apoptosis pathways, experimental perturbation of regulatory links between initiator and effector caspases reveals that XIAP and proteasome-dependent degradation of effector caspases are important in restraining activity during the pre-MOMP delay. We identify conditions in which restraint is impaired, creating a physiologically indeterminate state of partial cell death with the potential to generate genomic instability. Together, these findings provide a quantitative picture of caspase regulatory networks and their failure modes.

INTRODUCTION

Activation of initiator and effector caspases is a defining characteristic of apoptosis. Effector caspases cleave essential cellular substrates and directly dismantle cells, whereas initiator caspases have a more limited range of substrates and act primarily to regulate effector caspases (Fuentes-Prior and Salvesen, 2004). The precise, all-or-none control of caspase activation is critically important for control of cell fate: effector caspases must not turn on prematurely, but once active they must fully cleave their substrates and provoke cell death, lest cells survive with partially digested cellular contents and damaged genomes (Vaughan et al., 2002). Single-cell studies show that effector caspases are activated minutes before death but many hours after exposure to a death ligand (Goldstein et al., 2000; Rehm et al., 2002; Tyas et al., 2000). Little is known about the state of caspase regulatory networks during the long delay between receptor engagement and the induction of cell death, a significant gap in our understanding of the regulatory logic of apoptosis.

The chain of events that initiates extrinsic cell death begins with ligand-induced assembly of death-inducing signaling complexes (DISCs) on TNF, Fas, or TRAIL receptors (Kischkel et al., 1995; Martin et al., 1998). The initiator caspases-8 and -10 are activated by enforced dimerization at DISCs (Boatright et al., 2003; Donepudi et al., 2003), after which they cleave effector procaspases, causing a >100-fold increase in effector activity (Bose et al., 2003; Han et al., 1997). In the case of procaspase-3, activating proteolysis occurs at Asp175, separating the enzyme into large and small subunits that remain physically associated (Fuentes-Prior and Salvesen, 2004). Similar biochemistry is observed for intrinsic apoptosis after intracellular injury, except that caspase-9 is typically the initiator (Srinivasula et al., 1998). Effector caspases were once thought to autoactivate via homotypic procaspase cleavage, but recent work shows that this is not the case: the activation of procaspase-3 by proteolysis is mediated exclusively by initiator caspases (Liu et al., 2005). Subsequent to cleavage by initiators, effector caspases are regulated by *trans*-acting factors such as X-linked inhibitor of apoptosis protein (XIAP), which blocks the proteolytic activity of caspase-3 by binding tightly to its active site (Huang et al., 2001). XIAP may also encode an E3 ubiquitin ligase that promotes caspase-3 ubiquitination and its subsequent proteasome-mediated degradation (Chen et al., 2003; Suzuki et al., 2001).

In most cells (those with type-II regulation) (Scaffidi et al., 1998), XIAP-mediated inhibition of caspase-3 is relieved by a pathway that involves *m*itochondrial *o*uter *m*embrane *p*ermeabilization (MOMP) (Deng et al., 2002; Li et al., 2002; Sun et al., 2002; Zhang et al., 2001). MOMP is regulated by the Bcl-2 family of proteins, which functions either as proapoptotic (e.g., Bid or Bax) or antiapoptotic (e.g., Bcl-2) factors (Kim et al., 2006). Initiator caspases directly cleave Bid, which then activates Bax by altering its conformation (Eskes et al., 2000; Luo et al., 1998). Activated Bax translocates to the mitochondria, forming pores that allow Smac/Diablo and cytochrome *c* to translocate from their normal locations in the mitochondrial intermembrane space to the cytosol (Munoz-Pinedo et al., 2006; Oltvai et al., 1993). Smac binds tightly to XIAP, blocking XIAP's caspase-3-inhibitory activity (Du et al., 2000; Verhagen et al., 2000), whereas cytochrome *c* binds Apaf-1 and caspase-9 to form the apoptosome. Finally, in at least some cells, active caspase-3 cleaves procaspase-6, which then generates additional caspase-8 in a feedback

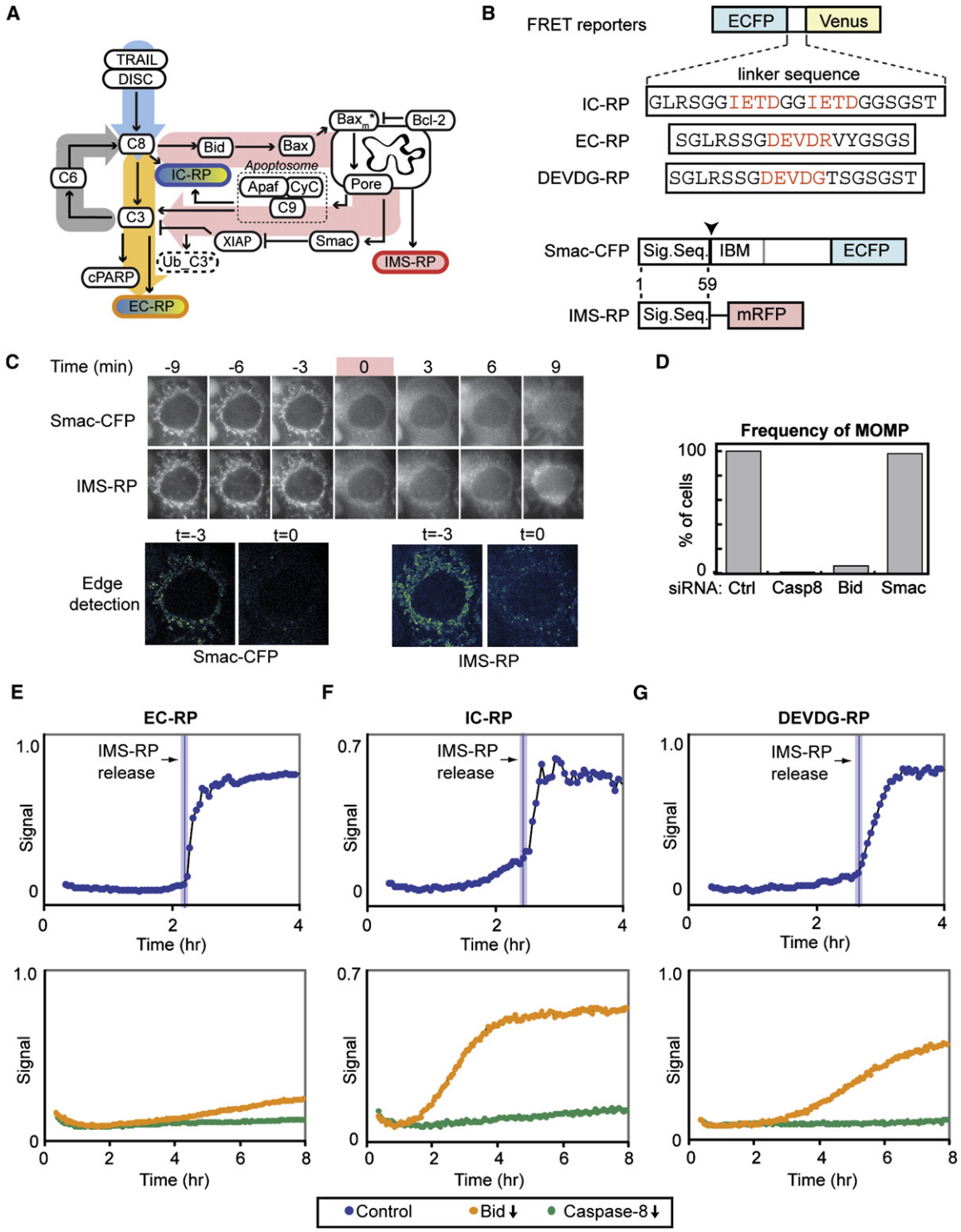

Figure 1. Live-Cell Reporters for Monitoring Extrinsic Cell Death

In all cases, cells were treated with 50 ng/ml TRAIL+2.5 μg/ml CHX.

(A and B) Schematic diagram of TRAIL-induced apoptotic pathways and reporter proteins. Abbreviations: ECFP, enhanced cyan fluorescent protein; Venus, Venus yellow fluorescent protein; Sig. seq., mitochondrial import signal sequence; IBM, IAP-binding motif; and mRFP, monomeric red fluorescent protein.

(C) Kinetics of IMS-RP and Smac-CFP release from mitochondria. Top, images from an individual cell expressing both IMS-RP and Smac-CFP and treated with TRAIL+CHX, at 3 min intervals. Time is relative to the first frame in which IMS-RP and Smac-CFP translocation was visible (t = 0, pink bar). Bottom, comparison of IMS-RP and Smac-CFP localization immediately before (t = −3 min) and after (t = 0 min) MOMP using an edge detection filter (see Experimental Procedures).

loop (Cowling and Downward, 2002; Murphy et al., 2004). Thus, the dynamics of extrinsic apoptosis are shaped to a lesser or greater degree by three cooperating but asynchronous processes: direct cleavage of effector caspases by initiators, cytosolic translocation of proapoptotic mitochondrial proteins, and feedback from effector to initiator caspases.

Live-cell reporters of caspase activity and MOMP reveal considerable heterogeneity in the dynamics of apoptosis from cell to cell within a population that is nominally genetically homogeneous (Goldstein et al., 2000; Munoz-Pinedo et al., 2006; Rehm et al., 2002, 2003; Takemoto et al., 2003; Tyas et al., 2000). Much of the heterogeneity is due to the variable delay, many hours in duration, between exposure to a proapoptotic stimulus and the sudden initiation of MOMP. This delay cannot be attributed solely to slow transcriptional processes, because it is observed even in the presence of drugs that block ongoing transcription or translation (Goldstein et al., 2000; Rehm et al., 2002). In this study, we examine the relative dynamics of initiator and effector caspase activation and MOMP by using four experimental tools: (1) live-cell reporters specific to initiator and effector caspases, (2) a biologically inert reporter of MOMP, (3) flow cytometry and immunoblot analysis of endogenous substrates, and (4) perturbation of specific proteins with RNAi, protein overexpression, and small molecule drugs. Analysis of initiator and effector caspase dynamics with a newly developed mathematical model of extrinsic apoptosis reveals a long-lived cellular state in which cleaved effector caspases are held safely in check while initiator caspases are active; failure to sustain this state makes the commitment to apoptosis ambiguous and yields damaged but undead cells with partly proteolyzed cellular contents.

RESULTS

Selective Live-Cell Reporters for Initiator and Effector Caspases

To monitor caspase regulation in single living cells, we constructed three fluorescent protein (FP) fusions (Figures 1A and 1B). The first, effector caspase reporter protein (EC-RP), monitors caspase-3 activity (and, to a lesser extent, caspase-7 activity) and is composed of a Förster resonance energy transfer (FRET) donor-acceptor pair (CFP and YFP) connected via a flexible linker that contains the caspase cleavage sequence DEVDR (Figure 1B). When the linker is cleaved, energy transfer is lost and the CFP signal increases, an event that can be monitored by live-cell microscopy. The DEVDR linker in EC-RP is expected to have 20-fold greater selectivity for caspase-3 relative to caspase-8 than the DEVDG linker used in previously published caspase reporters (Rehm et al., 2002; Tyas et al., 2000), based on in vitro data showing DEVDR to reduce k_{cat}/K_m for caspase-8 ~300-fold but k_{cat}/K_m for caspase-3 only ~14-fold relative to DEVDG (Stennicke et al., 2000).

Initiator caspase reporter protein (IC-RP) carries tandem copies of IETD in its linker, a sequence that is efficiently cleaved by caspase-8 (Luo et al., 2003) but poorly by caspases-3 and -7 (Thornberry et al., 1997). IETD constitutes the site in procaspase-3 for initiator caspase cleavage, and IC-RP cleavage is therefore a good readout of procaspase-3 activation. Finally, a reporter for MOMP that localizes to the mitochondrial *i*nter-*m*embrane space (IMS-RP) was created by fusing RFP to the mitochondrial import sequence of Smac (residues 1–59) (Du et al., 2000). FP fusions to full-length cytochrome *c* and Smac have been described previously (Goldstein et al., 2000; Munoz-Pinedo et al., 2006; Rehm et al., 2003), but IMS-RP differs from these fusions in that it is biochemically inactive, as it lacks an IAP-binding motif.

To validate the properties of EC-RP, IC-RP, and IMS-RP in vivo, HeLa cells stably expressing the reporter proteins were treated with TRAIL and cycloheximide (CHX), and fluorescence signals were monitored every 3 min over an 8–12 hr period. IMS-RP distribution was monitored with an image-processing algorithm that detects shifts from punctuate mitochondrial to diffuse cytosolic fluorescence. When cells were treated with varying doses of TRAIL, IMS-RP relocalized at the same time as a coexpressed Smac-CFP fusion (Karbowski et al., 2004) and ~6–9 min prior to the appearance of apoptotic cellular morphology (Figure 1C and Movie S1 available online). IMS-RP translocation was blocked in TRAIL-treated cells by RNAi-mediated depletion of caspase-8 and Bid, upstream components of the extrinsic cell death pathway, but not by RNAi of downstream components such as Smac (Figure 1D). Thus, IMS-RP appears to be a faithful reporter of protein translocation at MOMP, a process whose dynamics differs from that of falling mitochondrial membrane potential as measured with dyes (Munoz-Pinedo et al., 2006).

Caspase-mediated proteolysis of EC-RP and IC-RP was monitored by calculating the ratio of CFP and YFP emission, with suitable correction for background (see Experimental Procedures). Due to spectral overlap, it was not possible to monitor EC-RP, IC-RP, and IMS-RP fluorescence simultaneously in single cells, and we therefore expressed the reporters in pairs. When cells coexpressing EC-RP and IMS-RP were treated with TRAIL, increases in the CFP:YFP ratio resulting from reporter cleavage were sudden and took place only after IMS-RP translocation (Figure 1E; note that EC-RP signals were typically lost when cells detached from the slide subsequent to the appearance of apoptotic morphology). EC-RP cleavage was reduced 20-fold by RNAi of caspase-8 and 5-fold by RNAi of Bid, consistent with a requirement for MOMP in caspase-3 activation. Control experiments also established that changes in EC-RP fluorescence required TRAIL (CHX alone had no effect) and were sequence specific (being absent with a noncleavable DEVG-carrying reporter; Figure S1). However, changes in cell morphology did alter apparent FRET signals and were therefore taken into account during image analysis (see Supplemental Data).

Cells coexpressing IC-RP and IMS-RP exhibited gradual increases in IC-RP signal subsequent to TRAIL treatment and rapid increases subsequent to MOMP (IMS-RP release; Figure 1F). The early, gradual phase of IC-RP cleavage was insensitive to Bid depletion, but the fast post-MOMP phase was eliminated by it; both were blocked by depletion of caspase-8.

(D) Percentage of cells exhibiting IMS-RP release when transfected with control, Bid, caspase-8, or Smac siRNAs and treated for 12 hr with TRAIL+CHX.
(E–G) Time courses of cleavage for EC-RP (E), IC-RP (F), or DEVDG-RP (G) imaged in single siRNA-transfected cells treated with TRAIL+CHX. In cells treated with control siRNA, vertical lines indicate the time of IMS-RP release; release did not occur in the Bid- and caspase-8-depleted cells.

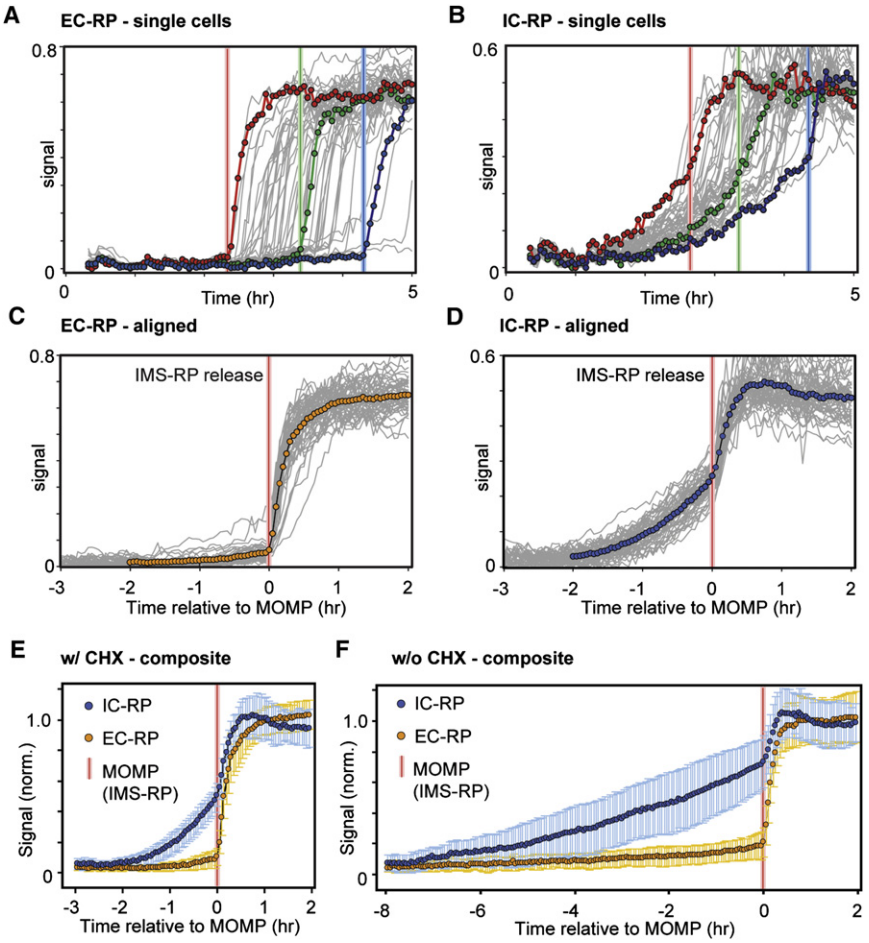

Figure 2. A Composite Picture of Effector and Initiator Caspases in Single Cells

(A and B) Time courses of cells expressing IMS-RP and either EC-RP (A) or IC-RP (B), treated with 50 ng/ml TRAIL and 2.5 μg/ml CHX. Fifty individual cells are shown for each reporter (gray lines), with three cells exhibiting early, late, or intermediate times of death highlighted in red, blue, and green; vertical bars indicate the time of IMS-RP release for each highlighted cell.

(C and D) EC-RP (C) or IC-RP (D) time courses from 50 single cells (in gray), aligned by IMS-RP release in each cell (red vertical line). Averaged signals for each reporter are shown as colored circles.

(E and F) Composite graphs of live-cell data for HeLa cells treated with 50 ng/mL TRAIL with (E) or without (F) 2.5 μg/ml CHX. For each treatment condition, average IC-RP (blue) and EC-RP (yellow) signals from >40 cells were aligned by IMS-RP release (red vertical line). Error bars indicate one standard deviation from the mean.

Rapid IC-RP cleavage post-MOMP probably reflects either elevated caspase-8 activity resulting from feedback via caspase-6 or cleavage by caspase-9 (RNAi experiments were ambiguous with respect to these possibilities, but the IETD sequence in IC-RP is known to be a good caspase-9 substrate). We therefore conclude that IC-RP is a selective readout of caspase-8 activity prior to MOMP but is unlikely to retain this selectivity later on; however, it is complemented by EC-RP, which is the key readout of the post-MOMP state. Direct comparison with a traditional reporter carrying a DEVDG caspase-3 recognition sequence further demonstrates the utility of the new EC-RP reporter: unlike EC-RP, or endogenous caspase substrates (see below), cleavage of the traditional reporter occurred prior to MOMP (as monitored by IMS-RP release) and was only partially blocked by Bid depletion (Figure 1G).

Initiator, but Not Effector, Caspase Activity in Pre-MOMP Cells

To derive a quantitative picture of caspase activation dynamics, the timing of cleaved IC-RP and EC-RP accumulation and of IMS-RP release from mitochondria were measured in 50–100 cells relative to the time of TRAIL addition (defined as t = 0; Figures 2A and 2B). Considerable cell-to-cell variability was observed in the time of IMS-RP release and the onset of EC-RP cleavage (from t ~1.5 to 4.5 hr), consistent with previous reports (Goldstein et al., 2000; Rehm et al., 2002). However, when live-cell movies were aligned based on the time of IMS-RP release, a clear picture of the progression in caspase activities emerged (Figures 2C–2E). In all cells, IC-RP cleavage rose slowly soon after TRAIL addition to ~50% of its maximum level at the time of IMS-RP release, after which the rate of cleavage increased substantially. At 50 ng/ml TRAIL, the pre-MOMP delay averaged 3.2 hr but could be as long as 12–24 hr at lower doses of TRAIL (Figures 2A and 2B and J.G.A., J.M.B., Sabrina L. Spencer, D.A.L., and P.K.S., unpublished data). In contrast, prior to IMS-RP release, the rate of EC-RP cleavage was very low, remaining at <5% of its maximum value and then rising rapidly over a 10–20 min period coincident with membrane blebbing and cell shrinkage, morphological manifestations of cell death (Figures 2A and 2C). Thus, subsequent to TRAIL addition but prior to MOMP (IMS-RP release), cells enter a "delay" state lasting several hours, during which initiator, but not effector, caspases are active (Figure 2E). The delay was even more pronounced in cells treated with TRAIL in the absence of CHX: in this case, IC-RP cleavage continued for longer and rose to substantially higher levels prior to IMS-RP release (~75% of maximum signal; Figure 2F). Moreover, delay was not restricted to signaling downstream of TRAIL receptors: even longer delays were observed in cells treated with TNF (data not shown).

Dynamics of Endogenous Caspase Substrate Cleavage

As assays for caspase activity, transfected reporter proteins have the drawback that they contain artificial cleavage sites

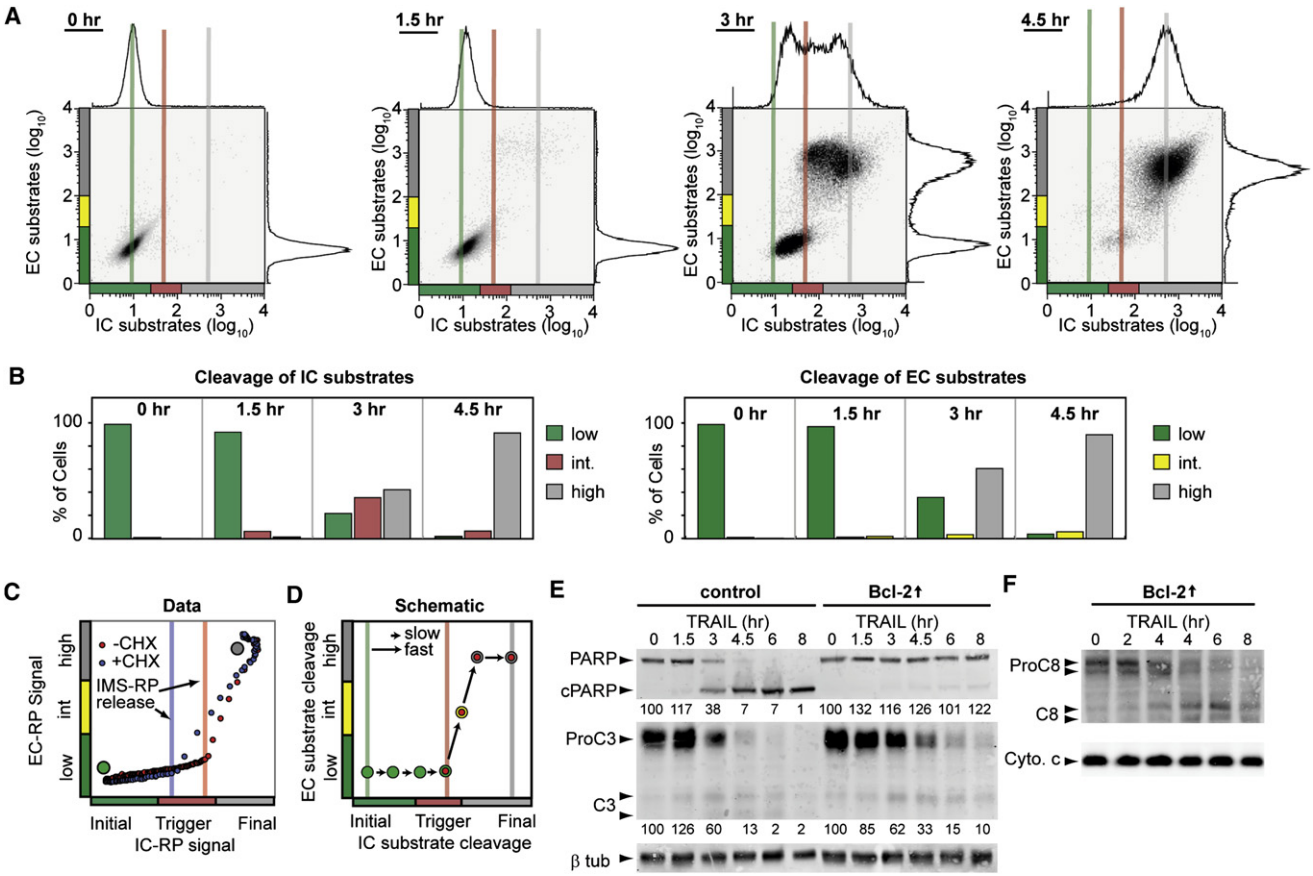

Figure 3. Input-Output Relationship between Initiator and Effector Caspases

(A) Flow cytometric detection of cleaved PARP (EC substrate) and cleaved caspase-3 (IC substrate) in HeLa cells treated with 10 ng/ml TRAIL and 2.5 μg/ml CHX. Single-parameter histograms derived from each 2D plot are shown above or to the right of the corresponding axes with colors denoting low (0%–5%), intermediate (5%–25%), and high (25%–100%) staining. Vertical lines denote thresholds of IC substrate cleavage as follows: green, median IC substrate signal in untreated cells; gray, median IC substrate signal in apoptotic cells; and red, threshold IC substrate level for transition from low to high EC substrate cleavage.

(B) Fraction of cells exhibiting low, intermediate, and high IC or EC substrate cleavage for the time course shown in (A) with identical color coding.

(C) Plot of input-output relationships between initiator and effector caspases derived from the live-cell data of Figures 2E and 2F. IC-RP and EC-RP signals at each time point are plotted directly against each other for cells treated with TRAIL in the presence (blue) or absence (red) of CHX; IMS-RP release is indicated by vertical lines.

(D) Schematic illustration of the sequence of initiator caspase (IC) and effector caspase (EC) substrate cleavage with circles denoting sequential states of the cell in response to TRAIL and arrows indicating the transition to the next state (with longer arrows indicating more rapid transitions). Circles are colored by the discretized level of EC substrate cleavage (corresponding to the colored bars on the vertical axis), with red dots indicating cells in which MOMP has occurred. Vertical lines denote the level of IC substrate cleavage in the initial state (green), final state (gray), and at the time of MOMP induction (red).

(E and F) Immunoblot detection of PARP, caspase-3, or caspase-8 processing for control or Bcl-2-overexpressing HeLa cells transfected with nontargeting siRNAs and treated with 50 ng/ml TRAIL + 2.5 μg/ml CHX for the indicated times.

and are overexpressed. To confirm that caspase dynamics measured with FPs were representative of endogenous caspase substrates, we turned to flow cytometry. Cleavage of initiator caspase substrates (designated IC substrates) was monitored with an antibody specific to a fragment of caspase-3 cleaved at Asp175 (the final residue in the IETD caspase-8 recognition site [Urase et al., 1998]), and cleavage of effector caspase substrates (EC substrates) was monitored with an antibody specific to cleavage of PARP at Asp214 by caspases-3 and -7 (Tewari et al., 1995). When cells harvested 0–4.5 hr after TRAIL addition were stained with both IC and EC cleavage-specific antibodies and examined by 2D flow cytometry, a broad distribution spanning ~10^2 fluorescence units was observed for IC substrate cleavage, whereas EC substrate cleavage was bimodal with clear negative (nonstaining) and positive (antibody-staining) peaks (see frequency distributions above and to the right of the scatter plots; Figure 3A). Discretization of the data into low, intermediate, and high levels revealed intermediate EC substrate cleavage to occur in less than 5% of cells, whereas intermediate IC substrate cleavage occurred in up to ~35% of cells (Figure 3B); however, the state of intermediate IC substrate cleavage was transient, eventually progressing to complete cleavage in all cells.

Comparison of flow cytometry and live-cell data was facilitated by plotting EC-RP and IC-RP fluorescence on a scatter plot (Figure 3C; note that, because both EC-RP and IC-RP

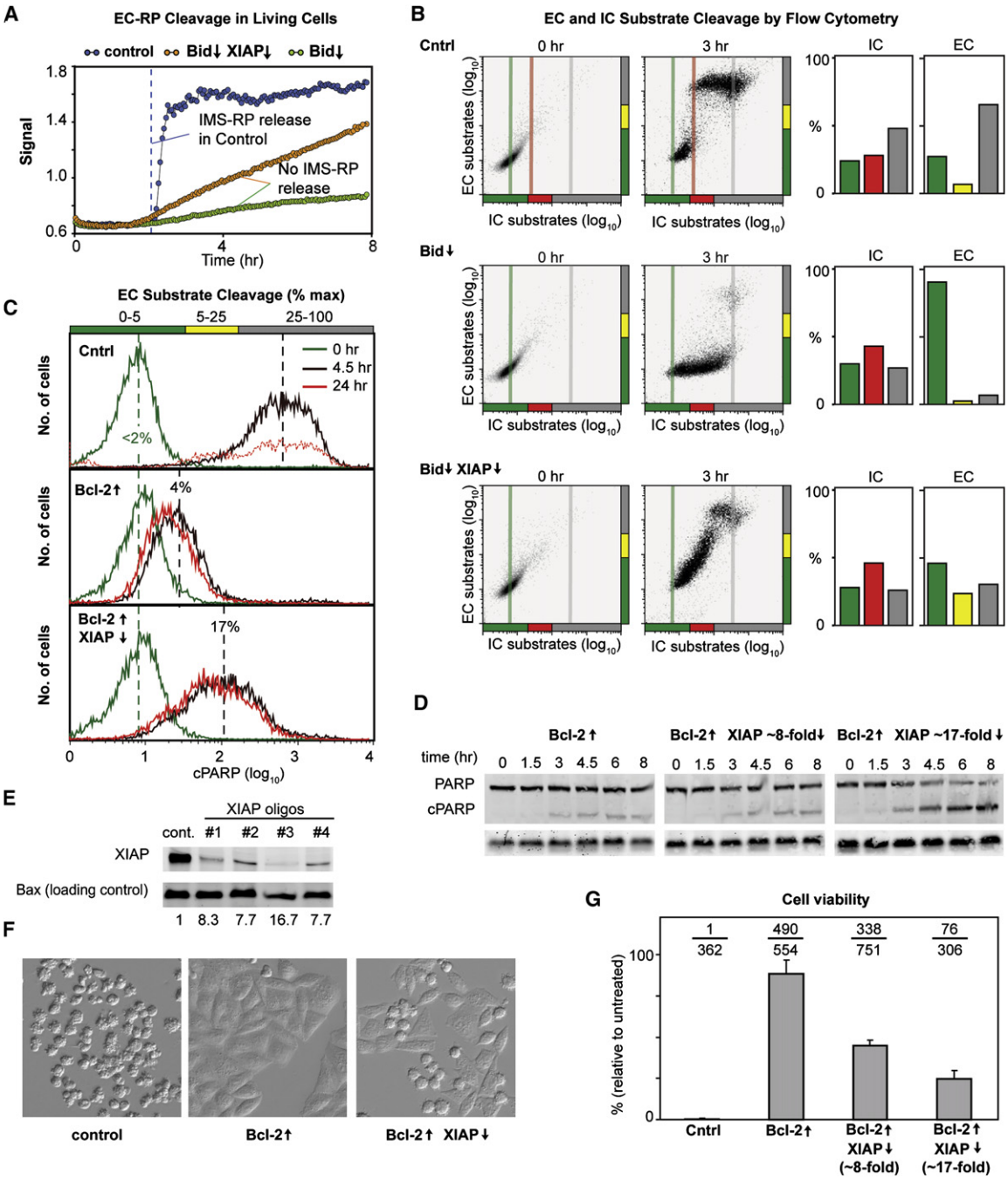

Figure 4. Breakdown of All-or-None Caspase Activation

In all cases, TRAIL was used at 50 ng/ml and CHX at 2.5 μg/ml.

(A) Time courses of EC-RP cleavage in single HeLa cells transfected with nontargeting (blue), Bid (green), or Bid plus XIAP (orange) siRNAs and treated with TRAIL+CHX.

(B) Flow cytometric detection of EC substrate (PARP) or IC substrate (caspase-3) cleavage in HeLa cells transfected with nontargeting, Bid, or Bid + XIAP siRNA oligos and treated with TRAIL+CHX. Plots are annotated as in Figure 3; bar graphs show the percentage of cells with low, medium, or high EC or IC substrate cleavage at 3 hr.

(C) Flow cytometric analysis of EC substrate cleavage in control and Bcl-2-overexpressing HeLa cells transfected with control or XIAP-targeting siRNAs and treated with TRAIL+CHX. Low, medium, and high PARP cleavage are indicated by colored bars, with dotted lines indicating the median fluorescence intensity of cleaved PARP at 4.5 hr; percentages are relative to control HeLa cells (set at 100%).

(D) Immunoblot detection of PARP cleavage for Bcl-2 overexpressing cells depleted 8- or 17-fold for XIAP with either of two siRNA oligos and treated with TRAIL+CHX. Results are representative of three independent experiments. β-tubulin is shown as a loading control (bottom panel).

signals increase monotonically, cells progress in time from lower left to upper right quadrants). A nonlinear input-output relationship between initiator and effector caspases was clearly evident regardless of the assay: imaging and flow cytometry both showed that EC substrate cleavage was low after TRAIL treatment but that IC substrate cleavage increased steadily until a threshold value was reached (red lines in Figure 3), at which point both IC and EC substrates were rapidly and fully processed (Figure 3C). Imaging showed that the transition to rapid cleavage coincided with IMS-RP release, and both assays agreed that the level of IC substrate cleavage at the MOMP transition was 1.5- to 2-fold higher in cells treated with TRAIL alone than in cells treated with both TRAIL and CHX (Figure S2).

As a final way to characterize the relationship between initiator and effector caspases, we used immunoblotting to examine procaspase-8, procaspase-3, and PARP cleavage after exposure to TRAIL. To make population-level measurements of pre-MOMP states possible, MOMP was blocked by overexpression of Bcl-2, a potent negative regulator of pore formation (Figure S3). Under normal conditions, >90% PARP was cleaved within 4.5 hr after TRAIL addition, but overexpression of Bcl-2 reduced PARP cleavage to <5% at 4.5 hr (Figure 3D). Nonetheless, procaspase-3 was processed with similar efficiency in both cases (Figure 3D), consistent with the kinetics of procaspase-8 cleavage and activation, which also proceeded to completion within 6 hr (Figure 3E). Thus, immunoblotting confirms the existence of a pre-MOMP state in which procaspase-8 processing leads to cleavage of procaspase-3, but the resulting cleaved caspase-3 does not proteolyze substrates such as PARP or cytokeratin.

Breakdown of All-or-None Caspase Activation

The absence of caspase-3 activity during the post-TRAIL, pre-MOMP waiting period implies the action of a potent inhibitor such as XIAP. We therefore expected that, in cells prevented from undergoing MOMP (by RNAi of Bid or overexpression of Bcl-2), depletion of XIAP would relieve caspase-3 inhibition. EC substrate cleavage was indeed restored under these conditions, but with a significant difference: cleavage of EC-RP lacked the delay period and sudden onset observed in control cells and instead rose gradually soon after TRAIL addition (Figure 4A). By flow cytometry, a breakdown in the normal input-output relationship between initiator and effector caspases was observed, with intermediate levels of EC substrate cleavage apparent in ~25% of cells (Figure 4B). Moreover, the extent of EC substrate cleavage did not increase between 4.5 and 24 hr, indicating that it had reached a steady state of 10%–20% processing (Figure 4C; this was more easily observed in the case of Bcl-2 overexpression than Bid depletion, presumably due to greater cell-to-cell uniformity in the former). The absence of ongoing EC substrate cleavage under these conditions was also confirmed by quantitation of cPARP levels on immunoblots (Figure 4D). Under these circumstances, the effects of XIAP depletion were found to be dose dependent: a second siRNA oligo that more efficiently reduced XIAP levels (17-fold versus 8-fold) increased the extent of EC-substrate cleavage (Figures 4E and 4F). Nonetheless, a sustained state of partial substrate cleavage, corresponding to ~50% PARP degradation, was still observed (Figure 4F).

To determine the consequences of partial EC substrate cleavage for cell fate, cells at t = 4.5 (with ~8-fold depletion of XIAP) were replated into fresh medium and the fraction of survivors found to be ~45% (Figures 4G and 4H; with ~17-fold depletion, ~25% of cells survived). We would expect such cells to suffer DNA damage via DFF40/caspase-activated DNase (CAD) (Samejima and Earnshaw, 2005), and increased levels of the DNA damage marker phospho-histone H2AX accompanied partial PARP cleavage (data not shown). However, we were unable to monitor DNA damage at the single-cell level and could not distinguish whether surviving cells (as opposed to those that die) sustain genomic damage. Nonetheless, it is clear that simultaneous disruption of MOMP and depletion of XIAP cause a dramatic failure in normal all-or-none commitment to cell death.

Mechanisms of "Partial" Cell Death

The observation that EC substrates can be cleaved to a steady submaximal level is surprising given the efficiency of caspase-3 as a protease. To understand how partial cleavage might arise and then persist, we turned to a mathematical model we had recently developed to describe reactions between TRAIL-receptor binding and cleavage of effector substrates (J.G.A., J.M.B., Sabrina L. Spencer, D.A.L., and P.K.S., unpublished data); the model includes (1) the direct action of caspase-8 on caspase-3, (2) induction of MOMP via competition among pro- and antiapoptotic Bcl-2 family proteins, and (3) caspase-6-mediated feedback between caspase-3 and caspase-8. The biochemistry of these processes is represented in the model by a set of elementary reactions that are cast as ordinary differential equations with parameter values derived from the literature or estimated by fitting to experimental data. Overall, the model accurately recapitulates the dynamics of extrinsic apoptosis in unperturbed and RNAi-treated single cells (see the Supplemental Data for details of model construction and validation). Model-based simulation serves as an effective tool for investigating quantitative relationships among cooperating and competing regulatory processes under various experimental conditions. By simulation, we found that even a tiny fraction of the procaspase-3 present in cells (1%, or ~10^2–10^3 molecules) (Stennicke et al., 1998) is sufficient to fully process EC substrates in several hours (Figure S4).

(E) Immunoblot quantitation of XIAP depletion by siRNA. HeLa cells were transfected with control or four different XIAP-targeting siRNA oligos for 48 hr and analyzed by immunoblot. Fold depletion of XIAP (relative to control oligo) is shown below each lane.

(F) Phase-contrast images of control or Bcl-2-overexpressing HeLa cells transfected with control or XIAP-targeting siRNA oligos and treated for 4.5 hr with TRAIL+CHX (conditions identical to those used in (C) and (D).

(G) Quantification of colony formation after TRAIL treatment. Control or Bcl-2 overexpressing cells were transfected with control or XIAP-targeting siRNA oligos. Fractions indicate the number of colonies formed after treatment with TRAIL+CHX (numerator) or with CHX alone (denominator); bars indicate the average percentage of colonies formed under TRAIL+CHX conditions normalized by the number formed under CHX alone. Error bars indicate one standard deviation from the average; results are representative of two independent experiments.

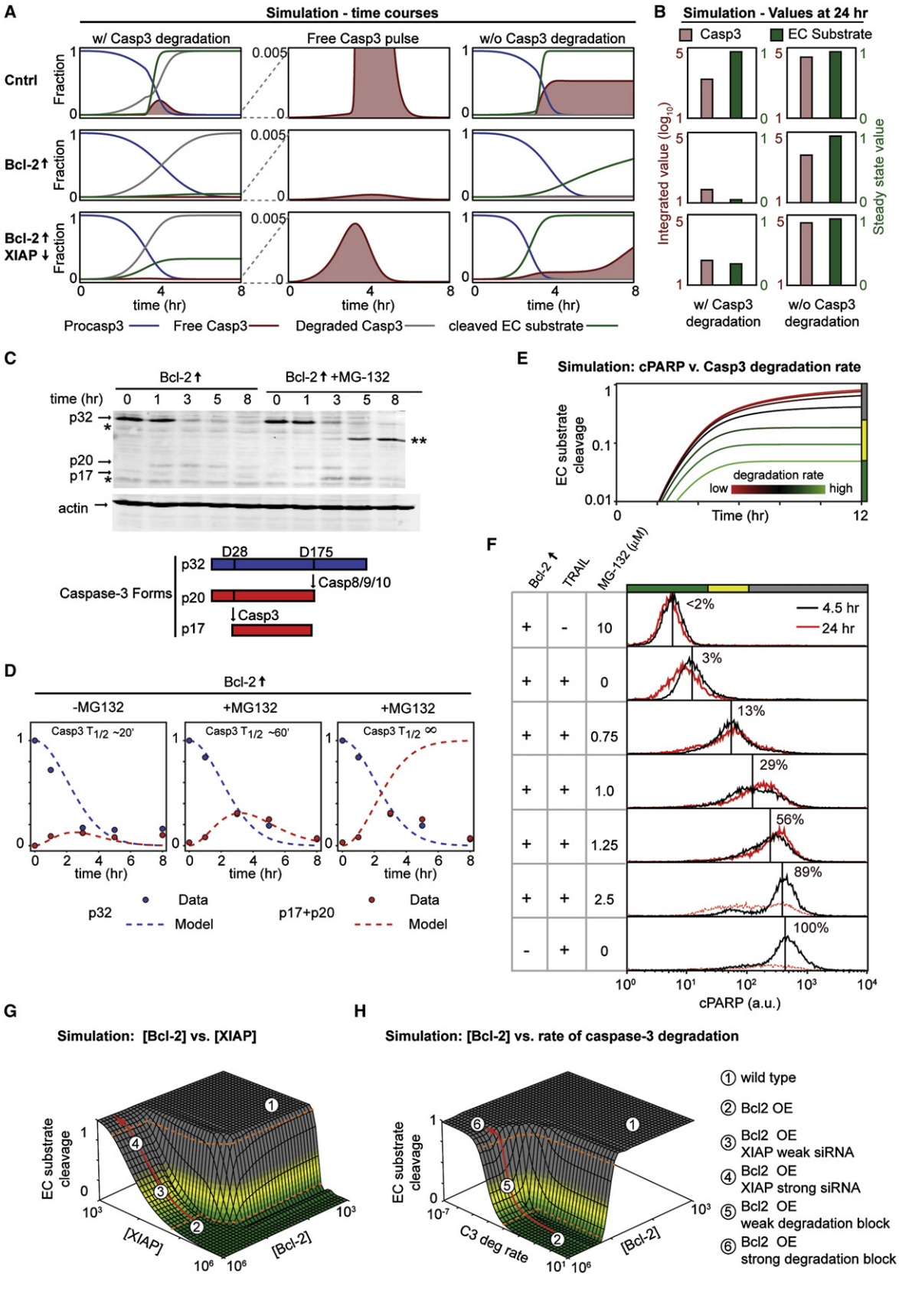
A
Simulation - time courses
w/ Casp3 degradation
Free Casp3 pulse
w/o Casp3 degradation
Cntrl
Bcl-2↑
Bcl-2↑ XIAP↓
Fraction
time (hr)
Procasp3
Free Casp3
Degraded Casp3
cleaved EC substrate
B
Simulation - Values at 24 hr
Casp3
EC Substrate
Integrated value (log10)
Steady state value
w/ Casp3 degradation
w/o Casp3 degradation
C
Bcl-2↑
Bcl-2↑ +MG-132
time (hr)
p32
p20
p17
actin
Caspase-3 Forms
D28
D175
Casp8/9/10
Casp3
D
Bcl-2↑
-MG132
+MG132
+MG132
Casp3 T1/2 ~20'
Casp3 T1/2 ~60'
Casp3 T1/2 ∞
time (hr)
p32
Data
Model
p17+p20
E
Simulation: cPARP v. Casp3 degradation rate
EC substrate cleavage
degradation rate
low
high
Time (hr)
F
Bcl-2↑
TRAIL
MG-132 (μM)
4.5 hr
24 hr
<2%
3%
13%
29%
56%
89%
100%
cPARP (a.u.)
G
Simulation: [Bcl-2] vs. [XIAP]
EC substrate cleavage
[XIAP]
[Bcl-2]
H
Simulation: [Bcl-2] vs. rate of caspase-3 degradation
EC substrate cleavage
C3 deg rate
[Bcl-2]
① wild type
② Bcl2 OE
③ Bcl2 OE XIAP weak siRNA
④ Bcl2 OE XIAP strong siRNA
⑤ Bcl2 OE weak degradation block
⑥ Bcl2 OE strong degradation block

However, when XIAP is present at normal levels in the model (corresponding to the optimum fitted value), caspase-3 catalytic activity is effectively restrained (Figure 5A). Critically, the model shows that partial EC substrate cleavage is absolutely dependent on the inactivation of caspase-3 soon after its production by initiator caspases; we had modeled this inactivation as proteasome and ubiquitin dependent based on previous reports (Chen et al., 2003; Suzuki et al., 2001) but without knowing its physiological significance. The onset of MOMP normally causes Smac to be released from mitochondria, sequestering XIAP and generating a pulse of caspase-3 far in excess of that required to cleave all EC substrates in the cell, regardless of whether or not caspase-3 is degraded (Figures 5A and 5B). When Bcl-2 is overexpressed or Bid depleted, thereby blocking MOMP, simulation shows that XIAP is present in excess over active caspase-3 and very little EC substrate is cleaved. However, when XIAP levels are reduced so as to simulate RNAi-mediated protein depletion, the direct action of caspase-8 on procaspase-3 serves as a limited source of caspase-3, which is then ubiquitinated and degraded. As a consequence, a pulse of active caspase-3 is generated whose limited duration results in cumulative caspase activity sufficient to cleave only a subset of the EC substrates present in a cell (~25% in the simulation in Figures 5A and 5B). The involvement, in simulation, of caspase-3 degradation in the pre-MOMP delay and partial EC substrate cleavage (Figures 5A and 5B) leads to two experimentally testable predictions: (1) when MOMP is blocked in TRAIL-treated cells, active caspase-3 should not accumulate due to ongoing proteasome-mediated degradation but should be stabilized in the presence of a proteasome inhibitor, and (2) increasing proteasome inhibition in pre-MOMP cells should result in increasing EC substrate cleavage.

Confirming the first prediction, immunoblotting with three different anti-caspase-3 monoclonal antibodies revealed that TRAIL-treated Bcl-2-overexpressing cells contained low levels of caspase-3 p20, an active form arising from cleavage of procaspase-3 at D175 by initiator caspases, and lacked detectable p17, which arises from autocatalytic cleavage of the p20 form (Figure 5C; epitope masking or destruction has previously been ruled out as a possible explanation for the phenomenon) (Tawa et al., 2004). Both p20 and p17 are active, but because generation of p17 requires caspase-3 catalytic activity, accumulation of p20 in the absence of p17 is characteristic of XIAP-mediated caspase-3 inhibition (Bratton and Cohen, 2003). In our experiments, the p17/p20 forms of caspase-3 were present at significant levels in extracts only when MG-132 was added at saturating concentrations (with p17 predominating, Figure 5C), consistent with the idea that p17/p20 destruction is proteasome dependent. When p32, p20, and p17 levels were quantified from western blot data, we estimated a p17/p20 half-life of ~20 min in the absence of MG132 and ~60 min in its presence (Figure 5D). These calculations are not straightforward because they must account for nonlinear production of p20 and p17 as procaspase-3 becomes depleted (see Supplemental Experimental Procedures), but we nonetheless conclude that caspase-3 is indeed degraded at a fairly rapid rate in pre-MOMP cells and that a significant fraction of this degradation is proteasome dependent. Substantially slower, proteasome-independent p17/p20 degradation is also evident, as suggested previously (Tawa et al., 2004).

To test the prediction that inhibiting proteasome activity not only promotes caspase-3 p17 accumulation but also induces EC substrate cleavage, Bcl-2-overexpressing cells were exposed to MG-132 for 30 min at concentrations spanning the drug's IC_{50}, and TRAIL was then added. Simulation showed that, under these conditions, levels of EC substrate cleavage at 24 hr (which approximates an end-point assay) should vary in a graded manner from partial to complete (Figure 5E). Flow cytometry of EC substrates strongly supported this prediction: as the concentration of MG-132 increased, the median level of substrate cleavage rose gradually from 5% to 89% (Figure 5F). Moreover, at low MG-132 concentrations, substrate cleavage ranged from 5% to 50% at 4.5 hr and no further increase was observed at 24 hr. When MG-132 exceeded 2 μM, however, substrate cleavage was extensive and many cells lysed, making the 24 hr time point unreliable (dotted lines in Figure 5F). Taken together, our data strongly support the hypothesis that

Figure 5. Mechanism of Partial Caspase-3 Substrate Cleavage

(A) Simulation of time evolution of procaspase-3, free (non-XIAP-bound) caspase-3, degraded caspase-3, and cleaved EC substrate for the indicated conditions; simulations are shown at full scale (first column) and at magnified scale to highlight low-abundance species (second column). The third column shows the same simulations performed in the absence of caspase-3 degradation. The area under the curve of free (non-XIAP-bound) caspase-3 is shaded pink to indicate the integrated total amount of caspase-3 activity in each condition.

(B) Correspondence of EC pulse size and steady-state EC substrate cleavage. For simulations of the conditions in (A), the integrated value of free active caspase-3 (maroon; shown on a $\log_{10}$ scale) and the final level of EC substrate cleavage (green) are shown for a period of 24 hr (to allow all species to reach steady state).

(C) Immunoblot with an anti-caspase-3 antibody in control cells treated with 50 ng/ml TRAIL+2.5 μg/ml CHX in the presence or absence of 10 μM MG-132. The diagram below the blot depicts the processing of the 32 kDa procaspase-3 to the active 20 kDa and 17 kDa forms; all three of these polypeptides are detected by the antibody used for the immunoblot (indicated by arrows). Single asterisk indicates nonspecific bands; double asterisks indicate a band whose identity is uncertain but whose size is consistent with monoubiquitinated caspase-3 p17.

(D) Estimation of cleaved caspase-3 stability. A simplified kinetic model was fit to quantitated immunoblot values in (C); see Supplemental Experimental Procedures.

(E) Simulation of PARP cleavage in Bcl-2-overexpressing cells with varying levels of XIAP-mediated caspase-3 degradation.

(F) Flow cytometric quantitation of cleaved EC substrate (PARP) in Bcl-2-overexpressing or control cells pretreated with varying concentrations of MG-132 and treated with 50 ng/ml TRAIL as indicated; all conditions included 2.5 μg/ml CHX. Vertical lines and percentages indicate the median EC substrate cleavage at 4.5 hr, relative to the level observed in control HeLa cells.

(G and H) Simulation of steady-state EC substrate cleavage as a function of Bcl-2 and XIAP levels ($[Bcl\text{-}2]_0$ and $[XIAP]_0$, in [G]) or as a function of $[Bcl\text{-}2]_0$ and the rate of caspase-3 degradation by XIAP (H). The height and color of the surface indicate the steady-state level of EC substrate cleavage for an idealized cell in response to TRAIL treatment; numbered circles correspond to the indicated experimental conditions. Red arrows show regions where partial EC substrate cleavage is induced by varying $[XIAP]_0$ (G) or rate of caspase-3 degradation (H).

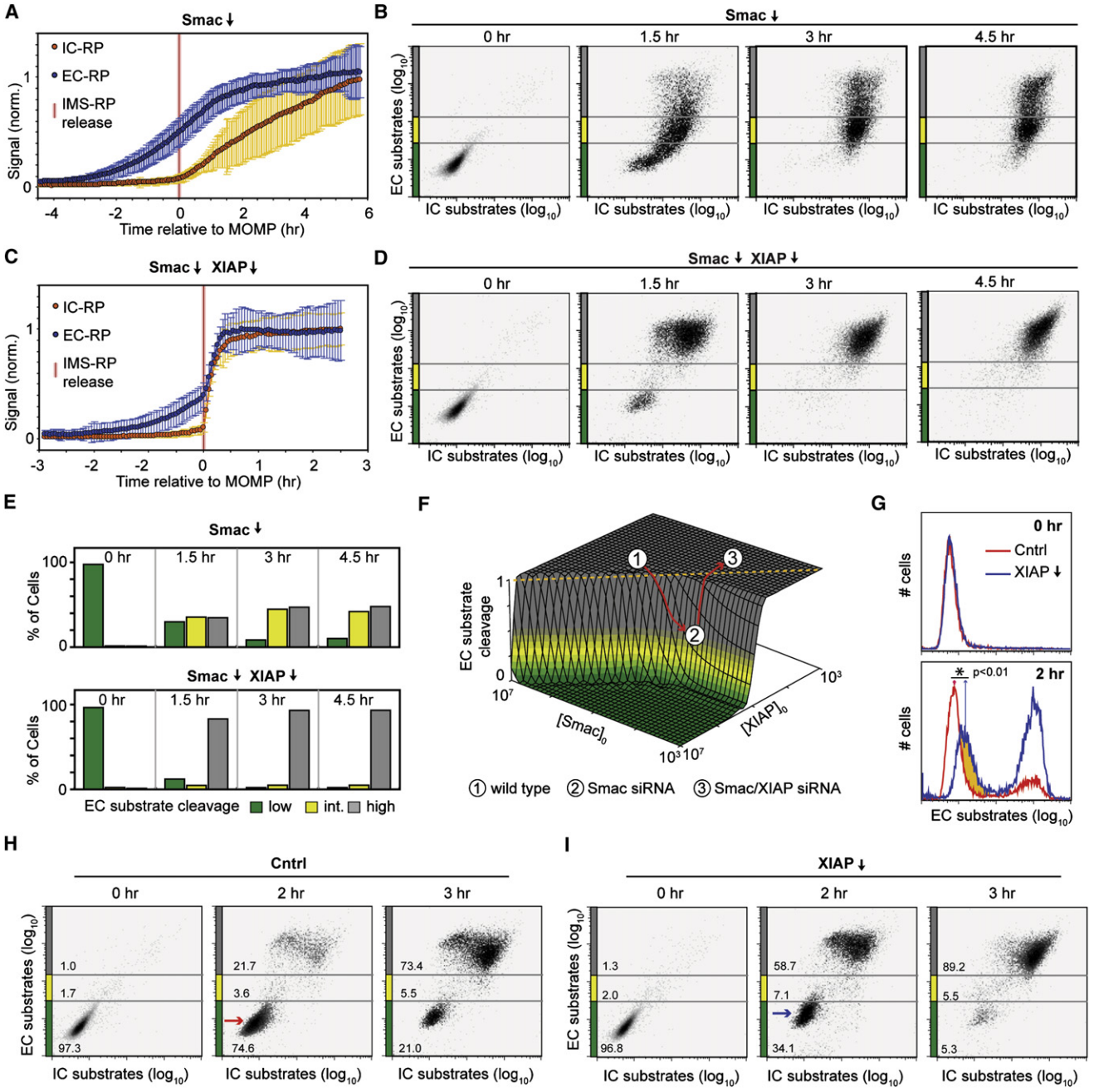

Figure 6. Importance of the Smac:XIAP Ratio for Rapid EC Substrate Cleavage

In all cases, TRAIL was used at 50 ng/ml and CHX at 2.5 μg/ml.

(A) Composite graph of single-cell initiator and effector caspase activity in Smac-depleted cells treated with TRAIL+CHX. Curves for EC-RP and IC-RP were assembled as in Figure 2 for n > 45 cells with each reporter; error bars indicate one standard deviation from the mean.

(B) Flow cytometry of cleaved EC substrate (PARP) and cleaved IC substrate (caspase-3) in Smac-depleted cells treated with TRAIL+CHX.

(C) Composite graph of IC-RP and EC-RP signals in Smac- and XIAP- depleted cells treated as in (A); error bars indicate one standard deviation from the mean.

(D) Flow cytometry analysis of Smac- and XIAP-depleted cells, as in (B).

(E) Fraction of cells exhibiting low, intermediate, and high EC substrate cleavage for the time courses shown in (B) and (D).

(F) Simulation of steady-state EC substrate cleavage as a function of initial expression levels of XIAP and Smac. Orange dotted line indicates the region where the initial concentrations of Smac and XIAP are equal.

(G) Comparison of cPARP levels in the pre-MOMP populations of control and XIAP-depleted cells. Arrows indicate the median cPARP levels for the pre-MOMP populations at 2 hr, which are different with $p < 0.01$ by the Komolgorov-Smirnov test (asterisk). The difference between the pre-MOMP populations for the two experimental conditions is highlighted in yellow.

ubiquitin-mediated caspase-3 degradation is essential for preventing EC substrate cleavage in pre-MOMP cells. The effects of perturbing Bcl-2, XIAP, and caspase-3 degradation can be viewed systematically in a bivariate landscape of predicted EC substrate cleavage relative to parameter values. Perturbations such as Bcl-2 overexpression shift cells away from a normal state characterized by rapid switching (position 1 in Figures 5G and 5H) to one in which EC substrate cleavage is strongly suppressed (position 2). This suppression by Bcl-2 overexpression is relieved by decreasing the level of XIAP (by RNAi) or the rate of caspase-3 degradation (by MG-132 treatment), resulting in a shift toward cell states characterized by slow and incomplete switching (positions 3 and 5) or a restoration of effective switching (positions 4 and 6).

Smac Translocation and XIAP Inactivation

Switch-like activation of caspase-3 under normal conditions requires rapid all-or-none inactivation of XIAP. RNAi-mediated depletion of Smac, the inhibitor of XIAP, should therefore interfere with caspase-3 activation and EC substrate cleavage. As expected, EC-RP cleavage was gradual in Smac-depleted cells (Figure 6A), and endogenous EC substrates were partially cleaved in >50% of cells at t = 4.5 hr (Figure 6B). Because Smac acts downstream of MOMP, partial EC-RP cleavage is observed only in Smac-depleted cells that have experienced MOMP (as measured by IMS-RP release, Figure 6A) and that are destined to die due to loss of normal mitochondrial function (Colell et al., 2007). Thus, "partial cell death" does not occur under these conditions. Remarkably, codepletion of XIAP and Smac restored normal caspase-3 activation as assayed by EC-RP cleavage and flow cytometry (Figures 6C–6E), suggesting that it is not the absolute levels of Smac and XIAP that are important but rather their ratio. Once again, the effects of perturbing Smac alone, or Smac/XIAP together, could be visualized on a bivariate landscape of EC substrate cleavage (Figure 6F).

The hypothesis that XIAP plays a critical role in controlling caspase-3 activity appears inconsistent with reports that apoptosis is regulated normally in XIAP knockout mice (Harlin et al., 2001). Cells in which XIAP had been depleted 8- to 17-fold by RNAi did exhibit responses to TRAIL similar to those of control cells, although with two subtle differences (Figure 6G–6I): (1) fully cleaved EC substrates appeared ~1 hr sooner, and (2) pre-MOMP cells exhibited small but reproducible increases in partial EC substrate cleavage (arrows in Figures 6G–6I). Upon subsequent onset of MOMP, this premature and partial substrate cleavage was overwhelmed by rapid activation of the bulk of caspase-3 and the phenotype therefore masked. The phenotypic consequences of XIAP depletion for initiator and effector caspase activation dynamics are therefore transient in our experiments, except when Bcl-2 is overexpressed or Bid depleted, preventing timely onset of MOMP.

DISCUSSION

In this paper we use live-cell imaging, flow cytometry, and mathematical modeling to examine the states of the core apoptotic network, comprising caspases and their immediate regulators, in HeLa cells exposed to TRAIL. Single-cell data show that cells treated with TRAIL enter a state of delay lasting many hours, during which initiator caspases are active (Figure 7A, state 2). Because procaspase-3 is a direct substrate of initiator caspases, the enzymatically active form of caspase-3 is generated steadily throughout the delay state, but its activity is held fully in check. Previous single-cell experiments examining the dynamics of initiator and effector caspase activation by death ligands have been contradictory, with the most recent reports concluding that the two are simultaneous (Kawai et al., 2004, 2005; Luo et al., 2003). Our data, based on improved reporters and quantitative analysis of a large number of cells, demonstrate that this is not the case. If MOMP is blocked by Bcl-2 overexpression or Bid depletion, or if TRAIL is added at very low doses, the pre-MOMP delay state can persist with initiator caspases on and effector caspases off for many hours (Figure 7A, state 2*).

Modeling and experiments reveal that, in the absence of new protein synthesis, maintaining a long-lasting pre-MOMP delay and then switching suddenly to rapid and decisive cell death places stringent demands on the pathways that regulate effector caspase activity. Caspase-3 is a very potent enzyme, and simulation shows that even ~400 active molecules are sufficient to cleave ~1 mg/ml cellular substrate (i.e., 10^6–10^7 molecules per cell) within several hours (Figure S4). Despite this catalytic efficiency, we observe that >90% of the 10^4–10^5 caspase-3 molecules present in a typical HeLa cell (Figure 3F) (Stennicke et al., 1998) are processed but held in check prior to MOMP without evidence of caspase-3-mediated EC substrate proteolysis. Experiments with proteasome inhibitors strongly suggest that ubiquitin-dependent degradation of caspase-3 is essential for effective inhibition of its enzymatic activity. Modeling reveals why this is true: were caspase-3 inhibition dependent solely on XIAP's activity as a nanomolar competitive inhibitor (K_d ~1 nM) (Huang et al., 2001), a >100-fold molar excess of XIAP over caspase-3 would be required to ensure the highly efficient inhibition of proteolytic activity observed experimentally in pre-MOMP cells (Figure S4). This arises because a competitive inhibitor of an irreversible enzymatic reaction must be present in large excess to block access of abundant substrates to the enzyme active site (Huang et al., 2001). However, XIAP is not present in large molar excess over caspase-3, and available data suggest that the proteins are present in HeLa cells at roughly similar levels (Rehm et al., 2006). Conversely, if caspase-3 is modeled as being unstable with a $t_{1/2}$ of ~20 min, active caspase never accumulates to a high level and the need for a vast excess of XIAP levels is reduced. XIAP has an E3 activity, and it is therefore reasonable to model it as having two activities, one as a competitive inhibitor of caspase-3 catalytic activity and the other as a mediator of XIAP ubiquitination (although other possibilities can be imagined, and direct tests with mutant XIAPs remain necessary). It should be noted that, even when both the competitive inhibitory and E3 ligase activities of XIAP are included in our model, the degree of caspase-3 inhibition observed in pre-MOMP cells is achieved only with XIAP levels higher than

(H and I) Flow cytometry of cleaved EC substrate (PARP) and cleaved IC substrate (caspase-3) in control and XIAP-depleted cells treated with TRAIL+CHX. Red and blue arrows indicate the pre-MOMP populations in control and XIAP-depleted conditions, respectively.

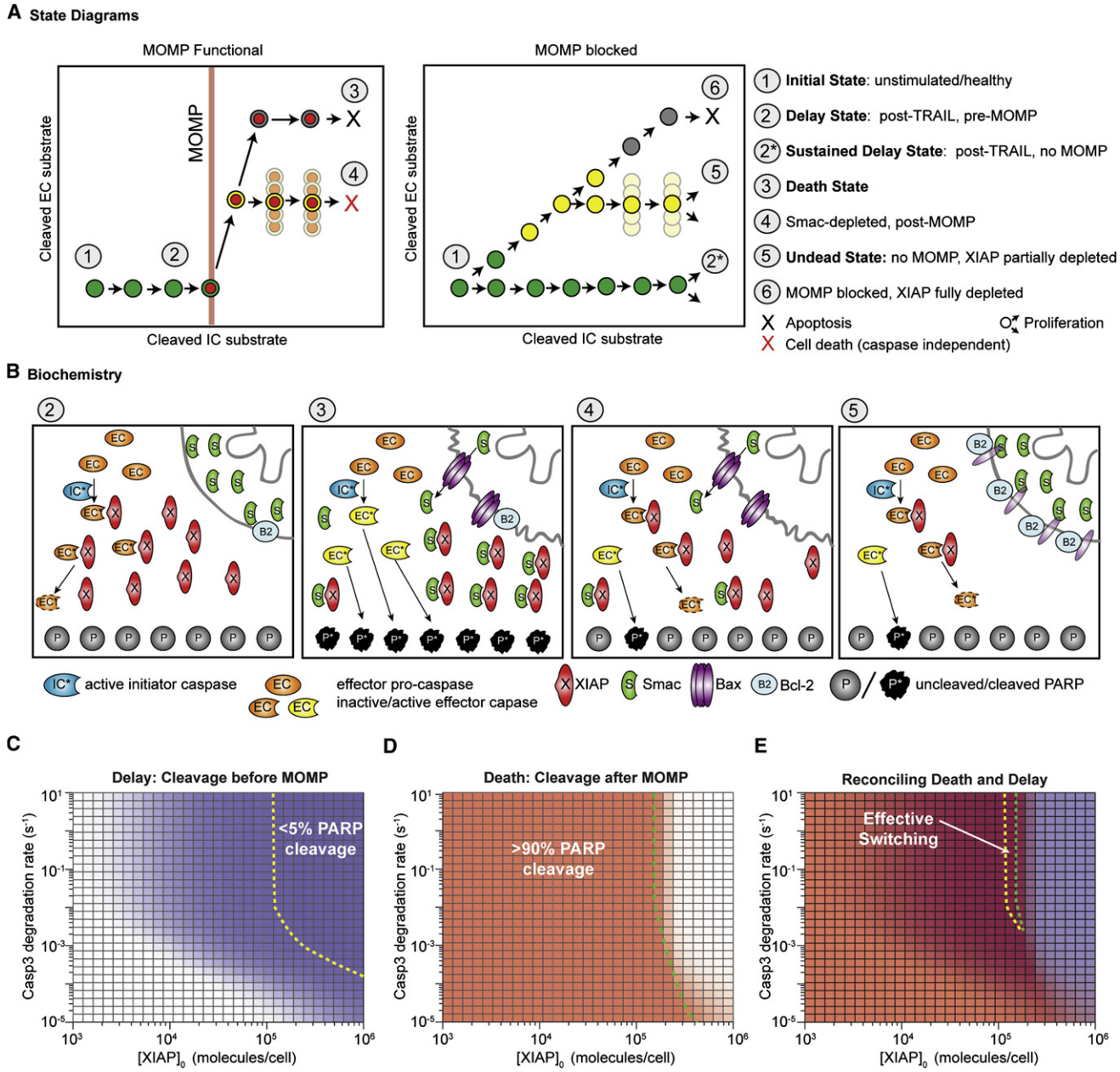

Figure 7. Constraints on XIAP for Effective Caspase-3 Switching

(A) Schematic diagrams depicting the progression of caspase network states in perturbed and unperturbed cells after TRAIL+CHX treatment. Diagrams are drawn according to the conventions in Figure 3C. The expected cell fate is depicted at the end of each progression as indicated in the legend.

(B) Graphical depiction of response to TRAIL stimulation in selected cell states, with numbering as in (A).

(C and D) Simulation of EC substrate cleavage in MOMP-inhibited cells as a function of initial XIAP concentration (horizontal axis) and the rate of caspase-3 degradation (vertical axis). Blue color in (C) indicates level of EC substrate cleavage at 6 hr, and the yellow dotted line denotes the region where the simulated cleavage level satisfies the experimentally observed constraint of <5%. Red color in (D) indicates the level of EC substrate cleavage at 6 hr, and the green dotted line denotes the region where the simulated cleavage level satisfies the experimentally observed level of >90%.

(E) Superposition of (C) and (D). Region bounded by yellow and green dotted lines encompasses parameter values that satisfy the constraints of both (C) and (D). Matlab scripts for each simulation are available in the Supplemental Data.

those estimated by quantitative western blotting (data not shown). Thus, additional mechanisms of caspase-3 inhibition are required, among which ubiquitin-independent caspase-3 degradation with a $t_{1/2}$ ~60 min is one (Figure 5D) (Tawa et al., 2004). Our working model is that three (and possibly more) distinct processes are involved in restraining caspase-3 catalytic activity during the pre-MOMP delay: competitive inhibition by XIAP, XIAP E3-mediated destruction by the proteasome, and

ubiquitin-independent proteolysis. Several developmental processes are associated with procaspase-3 cleavage in the absence of cell death, and it will be interesting to ascertain if similarly complex mechanisms of caspase-3 regulation are involved (Rosado et al., 2006).

Transitioning from a Pre-MOMP to a Dead State

In addition to maintaining a prolonged state of delay, a second fundamental challenge for the extrinsic cell death network is achieving a rapid and unambiguous transition to death (Figures 7A and 7B, state 3). In HeLa cells, this transition is dependent on MOMP. Our data support the widely held notion that a threshold level of proapoptotic Bcl-2 family proteins (such as tBid, the level of which is reflected by the level of IC-RP cleavage) must be reached for MOMP to occur and that the height of this threshold varies considerably depending on the physiological state of a cell. For example, we find that the MOMP threshold is 1.5- to 2-fold higher in the absence of CHX than in its presence, when assayed by IC-RP cleavage, a difference that we attribute in part to changes in the levels of the unstable Mcl-1 protein (data not shown). Once the threshold is reached, Smac is released into the cytosol, whereupon it binds to XIAP 3-fold more avidly than to XIAP binds to caspase-3 (Huang et al., 2001; Huang et al., 2003). Simulations show that the rapid 10-fold reduction in XIAP activity necessary for sudden and efficient EC substrate cleavage can be achieved assuming diffusion-limited binding and roughly equimolar XIAP and Smac. If we attempt to reconcile the demands of a stable delay (<5% EC substrate cleavage in pre-MOMP delay state, Figure 7C) with those of rapid and efficient transition to death (>90% EC substrate cleavage in the post-MOMP state, Figure 7D), the expression level of XIAP must lie within a relatively narrow range (Figure 7E). We anticipate that the precise shape of this landscape will differ among cell types, as CHX-treated HeLa cells used in this study are quite abnormal. Indeed, we have observed a different landscape of cellular states in Hct-116 cells (data not shown), although the model can be fitted to these data with a few adjustments to the expression levels of key proteins. Looking forward, it will be interesting to determine how the core apoptotic machinery is buffered against variation beyond the range of parameter values at which effective all-or-none switching is possible and whether a breakdown in switching is more frequent in disease.

Creating a State of Partial Cell Death

A third state of the caspase network, observed only in perturbed cells, involves persistent partial EC substrate cleavage (Figures 7A and 7B, states 4 and 5). If the extent of cleavage is insufficient (and our data suggest an LD_{50} for EC substrate cleavage of ~10% of full cleavage), cells survive despite damaged proteomes and genomes. DNA damage seems more likely to be pathological than protein degradation because it has the potential to cause genomic instability. Indeed, activation of effector caspases and downstream DNases in the absence of cell death has been proposed to induce the chromosomal translocations characteristic of leukemia (Betti et al., 2005; Vaughan et al., 2002, 2005; Villalobos et al., 2006). Our work identifies at least one way in which this state can arise through breakdown in pre-MOMP inhibition of caspase-3. Consistent with this finding, Bcl-2 is a potent oncogene in cancers such as leukemia that are characterized by chromosomal translocations (McDonnell and Korsmeyer, 1991). Perhaps the oncogenic effects of Bcl-2 reflect its ability to promote accumulation of genetic lesions via a malfunctioning apoptotic machinery as well as through its well- recognized ability to prevent apoptosis. The cooperation between Bcl-2 and MG-132, a drug similar in activity to the cancer therapeutic Bortezomib, in inducing a state of partial death further emphasizes the importance of understanding the responses of individual cells to perturbations in core apoptosis pathways. Avoiding physiologically indeterminate states of partial cell death is likely to be important in cancer treatment as well as in the normal physiology of programmed cell death.

EXPERIMENTAL PROCEDURES

Reporter Constructs

pECFP-Smac was obtained from Dr. Richard Youle. IMS-RP was constructed by PCR of bp 1-147 of Smac-1, ligation to the 5′ end of monomeric RFP-1, and cloning into pBabe-Puro. EC-RP, IC-RP, and DEVDG-RP were constructed by ligating Venus YFP between BamHI and EcoRI sites in pECFP-C1 and ligating linkers encoding cleavage sequences as BspEI-BamHI fragments between ECFP and Venus. Multiple serine and glycine residues flanking the cleavage sequences were added to increase linker flexibility and substrate accessibility.

Cell Lines and Materials

HeLa cells were obtained from the ATCC and cultured in DMEM supplemented with 10% calf serum and L-glutamine; Bcl-2-overexpressing cells were obtained from Dr. Fei Hua and Dr. Michael Cardone. HeLa cells stably expressing combinations of EC-RP, IC-RP, and IMS-RP were derived by transfection with FuGENE 6 (Roche) and isolation of puromycin and geneticin-resistant colonies. SuperKiller TRAIL was obtained from Alexis Biochemicals, CHX from Sigma-Aldrich, and MG-132 from Calbiochem. Flow cytometry, immunoblotting, colony forming assays, and computational modeling were performed by using conventional methods; see the Supplemental Data for details.

Live-Cell Microscopy and Image Analysis

Time-lapse movies were recorded with a Deltavision-modified Spectris IX71 fluorescence microscope equipped with an environmental chamber (Olympus, Applied Precision) at 10× or 60× magnification with frames every 3 min. Cells grown in 8-well chambered cover glass slides (Nunc) were shifted into phenol red-free CO_2-independent medium (Invitrogen) supplemented with 1% fetal bovine serum and L-glutamine for imaging. For FRET analysis, background-subtracted CFP and YFP images were divided to create a ratiometric image by using ImageJ and custom plug-ins (available on request). Signals were normalized by subtracting the minimum value across all time points from each single-cell time course. IMS-RP release was analyzed by edge detection in ImageJ or by visual inspection, which enabled an unambiguous identification of the first frame of IMS-RFP release in >95% of cells.

SUPPLEMENTAL DATA

Supplemental Data include Supplemental Experimental Procedures, Supplemental References, four figures, one table, two movies, and Matlab routines to reproduce all simulations in the paper and can be found with this article online at http://www.molecule.org/cgi/content/full/30/1/11/DC1/.

ACKNOWLEDGMENTS

We thank Dr. Fei Hua and Dr. Michael Cardone for Bcl-2-overexpressing HeLa cells and Dr. Richard Youle for kindly providing pECFP-Smac. We also thank R. Ward, S. Gaudet, S. Spencer, and D. Flusberg for helpful discussions. This work was supported by NIH grant P50-GM68762 to P.K.S. P.K.S. is a director of Applied PrecisionLLC, manufacturer of DeltaVision microscopes.

Received: September 27, 2007
Revised: December 14, 2007
Accepted: February 27, 2008
Published: April 10, 2008

REFERENCES

Betti, C.J., Villalobos, M.J., Jiang, Q., Cline, E., Diaz, M.O., Loredo, G., and Vaughan, A.T. (2005). Cleavage of the MLL gene by activators of apoptosis is independent of topoisomerase II activity. Leukemia *19*, 2289–2295.

Boatright, K.M., Renatus, M., Scott, F.L., Sperandio, S., Shin, H., Pedersen, I.M., Ricci, J.E., Edris, W.A., Sutherlin, D.P., Green, D.R., and Salvesen, G.S. (2003). A unified model for apical caspase activation. Mol. Cell *11*, 529–541.

Bose, K., Pop, C., Feeney, B., and Clark, A.C. (2003). An uncleavable procaspase-3 mutant has a lower catalytic efficiency but an active site similar to that of mature caspase-3. Biochemistry *42*, 12298–12310.

Bratton, S.B., and Cohen, G.M. (2003). Death receptors leave a caspase footprint that Smacs of XIAP. Cell Death Differ. *10*, 4–6.

Chen, L., Smith, L., Wang, Z., and Smith, J.B. (2003). Preservation of caspase-3 subunits from degradation contributes to apoptosis evoked by lactacystin: any single lysine or lysine pair of the small subunit is sufficient for ubiquitination. Mol. Pharmacol. *64*, 334–345.

Colell, A., Ricci, J.E., Tait, S., Milasta, S., Maurer, U., Bouchier-Hayes, L., Fitzgerald, P., Guio-Carrion, A., Waterhouse, N.J., Li, C.W., et al. (2007). GAPDH and autophagy preserve survival after apoptotic cytochrome c release in the absence of caspase activation. Cell *129*, 983–997.

Cowling, V., and Downward, J. (2002). Caspase-6 is the direct activator of caspase-8 in the cytochrome c-induced apoptosis pathway: absolute requirement for removal of caspase-6 prodomain. Cell Death Differ. *9*, 1046–1056.

Deng, Y., Lin, Y., and Wu, X. (2002). TRAIL-induced apoptosis requires Bax-dependent mitochondrial release of Smac/DIABLO. Genes Dev. *16*, 33–45.

Donepudi, M., Sweeney, A.M., Briand, C., and Grutter, M.G. (2003). Insights into the regulatory mechanism for caspase-8 activation. Mol. Cell *11*, 543–549.

Du, C., Fang, M., Li, Y., Li, L., and Wang, X. (2000). Smac, a mitochondrial protein that promotes cytochrome c-dependent caspase activation by eliminating IAP inhibition. Cell *102*, 33–42.

Eskes, R., Desagher, S., Antonsson, B., and Martinou, J.C. (2000). Bid induces the oligomerization and insertion of Bax into the outer mitochondrial membrane. Mol. Cell. Biol. *20*, 929–935.

Fuentes-Prior, P., and Salvesen, G.S. (2004). The protein structures that shape caspase activity, specificity, activation and inhibition. Biochem. J. *384*, 201–232.

Goldstein, J.C., Waterhouse, N.J., Juin, P., Evan, G.I., and Green, D.R. (2000). The coordinate release of cytochrome c during apoptosis is rapid, complete and kinetically invariant. Nat. Cell Biol. *2*, 156–162.

Han, Z., Hendrickson, E.A., Bremner, T.A., and Wyche, J.H. (1997). A sequential two-step mechanism for the production of the mature p17:p12 form of caspase-3 in vitro. J. Biol. Chem. *272*, 13432–13436.

Harlin, H., Reffey, S.B., Duckett, C.S., Lindsten, T., and Thompson, C.B. (2001). Characterization of XIAP-deficient mice. Mol. Cell. Biol. *21*, 3604–3608.

Huang, Y., Park, Y.C., Rich, R.L., Segal, D., Myszka, D.G., and Wu, H. (2001). Structural basis of caspase inhibition by XIAP: differential roles of the linker versus the BIR domain. Cell *104*, 781–790.

Huang, Y., Rich, R.L., Myszka, D.G., and Wu, H. (2003). Requirement of both the second and third BIR domains for the relief of X-linked inhibitor of apoptosis protein (XIAP)-mediated caspase inhibition by Smac. J. Biol. Chem. *278*, 49517–49522.

Karbowski, M., Arnoult, D., Chen, H., Chan, D.C., Smith, C.L., and Youle, R.J. (2004). Quantitation of mitochondrial dynamics by photolabeling of individual organelles shows that mitochondrial fusion is blocked during the Bax activation phase of apoptosis. J. Cell Biol. *164*, 493–499.

Kawai, H., Suzuki, T., Kobayashi, T., Mizuguchi, H., Hayakawa, T., and Kawanishi, T. (2004). Simultaneous imaging of initiator/effector caspase activity and mitochondrial membrane potential during cell death in living HeLa cells. Biochim. Biophys. Acta *1693*, 101–110.

Kawai, H., Suzuki, T., Kobayashi, T., Sakurai, H., Ohata, H., Honda, K., Momose, K., Namekata, I., Tanaka, H., Shigenobu, K., et al. (2005). Simultaneous real-time detection of initiator- and effector-caspase activation by double fluorescence resonance energy transfer analysis. J. Pharmacol. Sci. *97*, 361–368.

Kim, H., Rafiuddin-Shah, M., Tu, H.C., Jeffers, J.R., Zambetti, G.P., Hsieh, J.J., and Cheng, E.H. (2006). Hierarchical regulation of mitochondrion-dependent apoptosis by BCL-2 subfamilies. Nat. Cell Biol. *8*, 1348–1358.

Kischkel, F.C., Hellbardt, S., Behrmann, I., Germer, M., Pawlita, M., Krammer, P.H., and Peter, M.E. (1995). Cytotoxicity-dependent APO-1 (Fas/CD95)-associated proteins form a death-inducing signaling complex (Dros. Inf. Serv.C) with the receptor. EMBO J. *14*, 5579–5588.

Li, S., Zhao, Y., He, X., Kim, T.H., Kuharsky, D.K., Rabinowich, H., Chen, J., Du, C., and Yin, X.M. (2002). Relief of extrinsic pathway inhibition by the Bid-dependent mitochondrial release of Smac in Fas-mediated hepatocyte apoptosis. J. Biol. Chem. *277*, 26912–26920.

Liu, H., Chang, D.W., and Yang, X. (2005). Interdimer processing and linearity of procaspase-3 activation. A unifying mechanism for the activation of initiator and effector caspases. J. Biol. Chem. *280*, 11578–11582.

Luo, X., Budihardjo, I., Zou, H., Slaughter, C., and Wang, X. (1998). Bid, a Bcl2 interacting protein, mediates cytochrome c release from mitochondria in response to activation of cell surface death receptors. Cell *94*, 481–490.

Luo, K.Q., Yu, V.C., Pu, Y., and Chang, D.C. (2003). Measuring dynamics of caspase-8 activation in a single living HeLa cell during TNFalpha-induced apoptosis. Biochem. Biophys. Res. Commun. *304*, 217–222.

Martin, D.A., Siegel, R.M., Zheng, L., and Lenardo, M.J. (1998). Membrane oligomerization and cleavage activates the caspase-8 (FLICE/MACHalpha1) death signal. J. Biol. Chem. *273*, 4345–4349.

McDonnell, T.J., and Korsmeyer, S.J. (1991). Progression from lymphoid hyperplasia to high-grade malignant lymphoma in mice transgenic for the t(14; 18). Nature *349*, 254–256.

Munoz-Pinedo, C., Guio-Carrion, A., Goldstein, J.C., Fitzgerald, P., Newmeyer, D.D., and Green, D.R. (2006). Different mitochondrial intermembrane space proteins are released during apoptosis in a manner that is coordinately initiated but can vary in duration. Proc. Natl. Acad. Sci. USA *103*, 11573–11578.

Murphy, B.M., Creagh, E.M., and Martin, S.J. (2004). Interchain proteolysis, in the absence of a dimerization stimulus, can initiate apoptosis-associated caspase-8 activation. J. Biol. Chem. *279*, 36916–36922.

Oltvai, Z.N., Milliman, C.L., and Korsmeyer, S.J. (1993). Bcl-2 heterodimerizes in vivo with a conserved homolog, Bax, that accelerates programmed cell death. Cell *74*, 609–619.

Rehm, M., Dussmann, H., Janicke, R.U., Tavare, J.M., Kogel, D., and Prehn, J.H. (2002). Single-cell fluorescence resonance energy transfer analysis demonstrates that caspase activation during apoptosis is a rapid process. Role of caspase-3. J. Biol. Chem. *277*, 24506–24514.

Rehm, M., Dussmann, H., and Prehn, J.H. (2003). Real-time single cell analysis of Smac/DIABLO release during apoptosis. J. Cell Biol. *162*, 1031–1043.

Rehm, M., Huber, H.J., Dussmann, H., and Prehn, J.H. (2006). Systems analysis of effector caspase activation and its control by X-linked inhibitor of apoptosis protein. EMBO J. *25*, 4338–4349.

Rosado, J.A., Lopez, J.J., Gomez-Arteta, E., Redondo, P.C., Salido, G.M., and Pariente, J.A. (2006). Early caspase-3 activation independent of apoptosis is required for cellular function. J. Cell. Physiol. *209*, 142–152.

Samejima, K., and Earnshaw, W.C. (2005). Trashing the genome: the role of nucleases during apoptosis. Nat. Rev. Mol. Cell Biol. *6*, 677–688.

Scaffidi, C., Fulda, S., Srinivasan, A., Friesen, C., Li, F., Tomaselli, K.J., Debatin, K.M., Krammer, P.H., and Peter, M.E. (1998). Two CD95 (APO-1/Fas) signaling pathways. EMBO J. *17*, 1675–1687.

Srinivasula, S.M., Ahmad, M., Fernandes-Alnemri, T., and Alnemri, E.S. (1998). Autoactivation of procaspase-9 by Apaf-1-mediated oligomerization. Mol. Cell *1*, 949–957.

Stennicke, H.R., Jurgensmeier, J.M., Shin, H., Deveraux, Q., Wolf, B.B., Yang, X., Zhou, Q., Ellerby, H.M., Ellerby, L.M., Bredesen, D., et al. (1998). Procaspase-3 is a major physiologic target of caspase-8. J. Biol. Chem. *273*, 27084–27090.

Stennicke, H.R., Renatus, M., Meldal, M., and Salvesen, G.S. (2000). Internally quenched fluorescent peptide substrates disclose the subsite preferences of human caspases 1, 3, 6, 7 and 8. Biochem. J. *350*, 563–568.

Sun, X.M., Bratton, S.B., Butterworth, M., MacFarlane, M., and Cohen, G.M. (2002). Bcl-2 and Bcl-xL inhibit CD95-mediated apoptosis by preventing mitochondrial release of Smac/DIABLO and subsequent inactivation of X-linked inhibitor-of-apoptosis protein. J. Biol. Chem. *277*, 11345–11351.

Suzuki, Y., Nakabayashi, Y., and Takahashi, R. (2001). Ubiquitin-protein ligase activity of X-linked inhibitor of apoptosis protein promotes proteasomal degradation of caspase-3 and enhances its anti-apoptotic effect in Fas-induced cell death. Proc. Natl. Acad. Sci. USA *98*, 8662–8667.

Takemoto, K., Nagai, T., Miyawaki, A., and Miura, M. (2003). Spatio-temporal activation of caspase revealed by indicator that is insensitive to environmental effects. J. Cell Biol. *160*, 235–243.

Tawa, P., Hell, K., Giroux, A., Grimm, E., Han, Y., Nicholson, D.W., and Xanthoudakis, S. (2004). Catalytic activity of caspase-3 is required for its degradation: stabilization of the active complex by synthetic inhibitors. Cell Death Differ. *11*, 439–447.

Tewari, M., Quan, L.T., O'Rourke, K., Desnoyers, S., Zeng, Z., Beidler, D.R., Poirier, G.G., Salvesen, G.S., and Dixit, V.M. (1995). Yama/CPP32 beta, a mammalian homolog of CED-3, is a CrmA-inhibitable protease that cleaves the death substrate poly(ADP-ribose) polymerase. Cell *81*, 801–809.

Thornberry, N.A., Rano, T.A., Peterson, E.P., Rasper, D.M., Timkey, T., Garcia-Calvo, M., Houtzager, V.M., Nordstrom, P.A., Roy, S., Vaillancourt, J.P., et al. (1997). A combinatorial approach defines specificities of members of the caspase family and granzyme B. Functional relationships established for key mediators of apoptosis. J. Biol. Chem. *272*, 17907–17911.

Tyas, L., Brophy, V.A., Pope, A., Rivett, A.J., and Tavare, J.M. (2000). Rapid caspase-3 activation during apoptosis revealed using fluorescence-resonance energy transfer. EMBO Rep. *1*, 266–270.

Urase, K., Fujita, E., Miho, Y., Kouroku, Y., Mukasa, T., Yagi, Y., Momoi, M.Y., and Momoi, T. (1998). Detection of activated caspase-3 (CPP32) in the vertebrate nervous system during development by a cleavage site-directed antiserum. Brain Res. Dev. Brain Res. *111*, 77–87.

Vaughan, A.T., Betti, C.J., and Villalobos, M.J. (2002). Surviving apoptosis. Apoptosis *7*, 173–177.

Vaughan, A.T., Betti, C.J., Villalobos, M.J., Premkumar, K., Cline, E., Jiang, Q., and Diaz, M.O. (2005). Surviving apoptosis: a possible mechanism of benzene-induced leukemia. Chem. Biol. Interact. *153–154*, 179–185.

Verhagen, A.M., Ekert, P.G., Pakusch, M., Silke, J., Connolly, L.M., Reid, G.E., Moritz, R.L., Simpson, R.J., and Vaux, D.L. (2000). Identification of DIABLO, a mammalian protein that promotes apoptosis by binding to and antagonizing IAP proteins. Cell *102*, 43–53.

Villalobos, M.J., Betti, C.J., and Vaughan, A.T. (2006). Detection of DNA double-strand breaks and chromosome translocations using ligation-mediated PCR and inverse PCR. Methods Mol. Biol. *314*, 109–121.

Zhang, X.D., Zhang, X.Y., Gray, C.P., Nguyen, T., and Hersey, P. (2001). Tumor necrosis factor-related apoptosis-inducing ligand-induced apoptosis of human melanoma is regulated by smac/DIABLO release from mitochondria. Cancer Res. *61*, 7339–7348.